# Multifunctional aluminium surfaces – Laser-structured micropatterns with ice-repellent, superhydrophobic and easy-to-clean properties

*Stephan* Milles[1,*], *Marcos* Soldera[1,2], *Bogdan* Voisiat[1] and *Andrés Fabián* Lasagni[1,3]

[1] Institute of Manufacturing Science and Engineering, Technische Universität Dresden , Dresden, Germany
[2] PROBIEN-CONICET, Universidad Nacional del Comahue, Department of Electrical Engineering, Neuquén, Argentina
[3] Fraunhofer Institute for Material and Beam Technology IWS, Dresden, Germany

**Abstract.** In this work, the fabrication of multifunctional periodic microstructures on pure aluminium is presented. Three different geometries were fabricated with feature sizes ranging between 7 µm and 50 µm by using laser-based microstructuring methods. In detail, nanosecond pulsed direct laser writing and picosecond pulsed direct laser interference patterning were used with infrared laser radiation. The wetting characteristics of these structures were investigated performing static water contact angle measurements as well as by measuring the contact angle hysteresis and the sliding angle. The final wetting results show constant static contact angles above 150°, permitting the water droplets to roll off the substrate as well as collecting contamination at the same time. This self-cleaning effect led to a reduction of up to 94% of the spread of 1 µm sized manganese oxide particles. In addition, the freezing time required for droplets laying on the patterned surfaces was increased nearly by 300% at a temperature of 20 °C below zero. Finally, the results are compared to finite element simulations of heat transfer.

## 1 Introduction

A water droplet that is rolling off a slightly tilted surface is an outcome of the surface chemistry and topography as it was already observed on the lotus flower (nelumbo nucifera) many years ago [1]. This so-called superhydrophobic property results in many beneficial characteristics like high corrosion resistance, ice-repellence and self-cleaning, which gained an increasing demand for many industrial markets like the aviation, automotive, food or cooling industries [2]. A frequently used material in these fields is aluminium, as well as its alloys, due to its high strength and low weight [3].
Today, there is a wide variety of methods to modify the chemistry and/or topography in order to fabricate superhydrophobic surfaces on aluminum. For instance, by chemical etching (where the substrates are processed by a multi-step process in different acid baths), applying a silane coating onto the substrate or by micro-structuring the material using cutting tools like disk cutters [4–6]. In particular, water-repelling and self-cleaning surface are interesting for the food industry, where chemical cleaning should be avoided for hygienic reasons. On technical surfaces, pollution and sand particles can lead to increased wear of the components [7]. Therefore, a self-cleaning surface capable to remove particles from its surface by rinsing droplets and without applying any additional cleaning agents is beneficial. Besides that, not all superhydrophobic surfaces present an ice-repellent function [8]. The characteristic of preventing the formation of ice on the surface can be for instance achieved by thermo-mechanical treatments [9,10].

Besides the above mentioned surface treatments, laser technology presents a promising alternative to create a functional surface. Using Direct Laser Writing (DLW) well-defined surface topographies can be produced by ablating the material locally using a single laser beam which is focused on the material surface [11]. Due to the focusing limitations of the beam, the resolution of the fabricated patterns is usually restricted down to 10-20 µm, depending on the laser wavelength, focusing objectives and beam diameter.
An alternative method to fabricate surface patterns on a metallic surface with a resolution below 10 µm is Direct Laser Interference Patterning (DLIP). In this case, a single laser beam is divided into at least two beams which are overlapped on the surface of the material. If two laser beams are used, this leads to the formation of a line-like periodic intensity distribution, with an spatial period $\Lambda$ (repetitive distance between the interference maxima or minima) that can be calculated using Equation 1:

$$\Lambda = \lambda / [2 \sin (\beta /2)], \quad (1)$$

where $\lambda$ is a wavelength of the used laser radiation and $\beta$ is the angle between two interfering beams.

* Corresponding author: stephan.milles@tu-dresden.de

The geometry of the produced pattern depends on the number of overlapping beams [12,13]. The DLIP technology has been already used in a broad variety of applications due to the flexibility of materials that can be treated as well as the different patterns that can be created. For example, DLIP was used for manufacturing holographic structures as well as for producing security elements or textured surfaces for antibacterial applications [14–16]. However, to the best of our knowledge, there is a lack of research in the field of multifunctional microstructures on Al surfaces fabricated with laser-based methods, which includes three functionalities, namely superhydrophobicity, self-cleaning, and anti-icing.

In the presented study, we utilized DLW and DLIP technologies to create three different types of periodic structures. Nanosecond pulsed DLW is used for producing a mesh-like geometry with a feature size of 50 µm. In addition, picosecond two-beam DLIP is implemented for the fabrication of pillar-like structures with a spatial period of 7 µm. For producing a hierarchical structure, both technologies are combined. The time-dependent wetting characteristic of the microstructures is investigated by water contact angle measurements for 36 days together with the contact angle hysteresis and the sliding angle. The self-cleaning efficiency is investigated by an self-developed optical evaluation method. The influence of the microstructure on the icing-process is also examined under temperature conditions of -20°C. Finally, the experiments are additionally supported by finite element method simulations [17,18].

## 2 Materials and methods

### 2.1 Material

Samples consisting of pure aluminum 99.5 % (EN AW-1050) were used in this study. The sheets were electrolytically polished before the laser treatment obtaining a surface roughness (RMS) of 101 nm ± 10 nm.

### 2.2 Laser microstructuring procedure

For DLW, a workstation (GF machining solutions P 600) equipped with an Ytterbium fiber laser emitting at 1064 nm wavelength radiation with a maximal output power of 30 W was utilized. The pulse duration was set to 14 ns and the used repetition rate was 30 kHz. The beam was guided by an optical scanner with a speed of 250 mm/s and focused by a 254 mm focal length f-theta objective resulting in a focal diameter of 70 µm on the aluminium surface. The applied laser fluence was 1.1 J/cm². The fabricated mesh-like structure consists of three consecutively formed line-like structures, whose orientation is rotated by 60° respectively to each other. The distance between the lines was set to 50 µm [17].
The DLIP technology was applied to fabricate periodic 7 µm pillar-like structures, utilizing a solid-state Nd:$YVO_4$ laser (Edgewave PX 200, Germany) emitting 1064 nm wavelength with 10 ps pulse duration. The repetition rate was 30 kHz with a maximum output power of 10 W. The system is equipped with a commercial available DLIP optical head (manufactured by Fraunhofer IWS, Germany). Using this head, the line-like intensity profile, which extends over a circular shaped area with a diameter of ˜ 140 µm, is created [17]. The laser fluence was set to ~ 1.9 J/cm². In order to pattern larger areas, the sample was moved in x- and y-directions by using high-precision stages (Aerotech, USA) with an accuracy of ± 2.5 µm. In order to obtain pillar-like structures, the samples had to be structured twice by rotating the sample at 90° between the processing steps. Further information about the procedure has been published elsewhere [18,19].
The hierarchical DLW+DLIP structures were manufactured in a two-step process where the previously mentioned technologies were combined and conducted subsequently.

### 2.4 Surface characterization

The topography of the processed samples was analyzed using confocal microscopy with an 150x objective (Sensofar S Neox, Spain), resulting in 2 nm and 140 nm vertical and lateral resolutions, respectively. Scanning Electron Microscopy were also used (ZEISS Supra 40VP, Germany) at an operating voltage of 5.0 kV.

The static water contact angle (WCA), contact angle hysteresis (Hys) and sliding angle (SA) measurements were performed using a contact angle system (Krüss DSA 100 S, Germany), which is equipped with a special temperature chamber (Krüss TC40, Germany) based on a Peltier-element. For the measurements, 8 µl droplets of deionized water were used. The static water contact angles were calculated using the Young - Laplace and the tangent drop profile fitting methods and each point is the average of five measurements. In all experiments, the droplets were positioned automatically on the surface. For the ice-repellence tests at -20 °C, the freezing process was monitored and recorded by a CCD camera with a frame rate of 50 fps [18].

The heat transfer between the cold surface and the textured Al surface was simulated using finite element method with a commercial software (COMSOL Multiphysics 5.3.). More details regarding the simulation can be found in [18]. This model approach has been compared with the results of the experiments. The simulations are well suited for a deeper understanding of the heat flux between the different layers, namely the cold aluminium surface, the air inclusions due to the microstructure and the water droplet. However, they are limited with respect to the influence of thermal conductivity before and after the laser processing.

The self-cleaning functionality was evaluated using a self-developed setup including a CCD camera. 10 µl deionized water droplets were released at a tilting angle of 15° on the laser-treated substrates which were contaminated with 1 µm manganese oxide particles ($MnO_2$). Then, a picture was taken after every single droplet and the number of remaining particles on the

area of interest on the specimen was calculated using a image analysis software (ImageJ, Version 1.52a) [20].

## 3 Results and discussion

For investigating various topographies with specific feature sizes regarding their wettability, self-cleaning and the ice-repellent properties, three different textures were produced. In the following section, the fabrication of these patterns is described in detail, namely, (i) mesh-like structure fabricated using DLW, (ii) pillar-like structure fabricated by DLIP and (iii) a hierarchical multiscaled structure fabricated combining of DLW and DLIP.

### 3.1. Fabrication of periodic structures using DLW and DLIP technology

Mesh-like structures with a feature size of 50 µm were fabricated on Al substrates using DLW technology, based on a comprehensive previous study [17]. The scanning electron microscope (SEM) image (Fig. 1a) shows a homogeneous distributed pattern in which the third scanned line-like structure is dominant. The confocal microscope (CF) image, presented as an insert in Fig. 1a, reveals the topography of the structure, which shows on average a structure depth of 36.2 µm. This texture emerges due to the nanosecond-pulsed laser process, where the thermal diffusion length for aluminum is in the µm-range, leading to an increase of molten material and in consequence to the deep structures in this order of magnitude [21,22].

Later, the DLIP technology was used for producing significantly smaller structures compared to the previous described mesh-like pattern[23]. In order to produce 7 µm pillar-like structures with a two-beam interference setup, the sample was irradiated twice, with a 90° rotation between the irradiation steps [19]. Due to the pulsed manufacturing process, large areas can be processed as shown in Fig. 1b. The resulting structure depth was in this case 4.5 µm on average (Fig. 1b). In contrast to the ns-pulsed DLW process, the DLIP structures were fabricated utilizing a picosecond-pulsed (ps) laser which provides a thermal diffusion length in the nm-range. As a result the amount of molten and recasted material is significantly reduced [24].

Finally, both above-described technologies were combined for fabricating a multiscale hierarchical pattern. Applying the same process parameters, the substrate was firstly irradiated with DLW (50 µm mesh-like) and afterward using DLIP (7.0 µm pillar-like) resulting in the structure depicted in Fig. 1c. In the image it is also shown, that the facets of the DLW structure were not significantly ablated by the DLIP process due to their steep slope (see arrow in Fig. 1c). The resulting topographies were evaluated by CF microscopy and revealed structure depths of 33.8 µm for the DLW structures and ~4.2 µm for the DLIP structures situated on top of DLW structure (insert Fig. 1c).

### 3.2. Wetting characteristics

For examining the wetting characteristics of the three fabricated structures measurements of the static water contact angles (CA), the contact angle hysteresis (Hys) and the sliding angle were performed. In general, wetting is roughly divided into three regimes: hydrophilic (is defined by CAs below 90°), hydrophobic (describes the range between 90° and 150°) and superhydrophobic (represents CAs above 150°) [25].

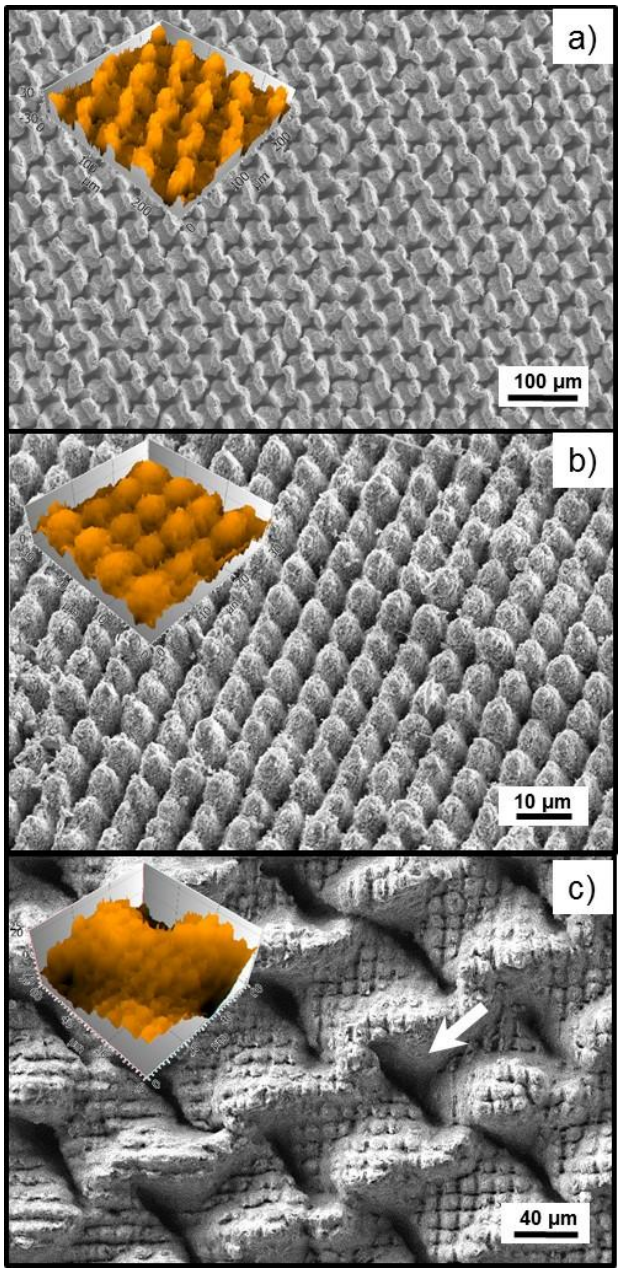


**Fig. 1.** SEM images of (a) mesh-like DLW structures with a feature size of 50 µm The utilized laser fluence was 1.1 J/cm², 14 ns pulse duration, 30 kHz repetition rate and the scan speed was 250 mm/s. Ten scan repetitions were used. (b) Pillar-like DLIP structures with a spatial of 7.0 µm fabricated with a fluence of 1.9 J/cm², a pulse overlap of 99% and a repetition rate of 1 kHz. (c) Hierarchical structure fabricated by combining DLW+DLIP. The laser wavelength for all experiments was 1064 nm. Confocal images of each structure are given in the top left corner, respectively.

The treated Al surfaces using DLW, DLIP and DLW+DLIP sand an untreated reference were constantly characterized during 36 days period. The obtained results are shown in Fig. 2a. The untreated reference presented a constant wetting characteristic with a CA of ~93° (see lower insert in Fig. 2a), which is common in aluminum surfaces [17,26]. In contrast, it was observed that all laser-treated substrates showed a constant increase in the CAs with time.

The initial low CA can be explained due to a significant change of the surface chemistry after the laser treatment. Then, the increase of carbon content at the Al-surface led to an increase of non-polar sites and thus to the raising of CA [27,28]. Later, the substrates became all hydrophobic and turned to a steady superhydrophobic state with a CA higher than 151° after 13 days (see upper insert Fig. 2a).

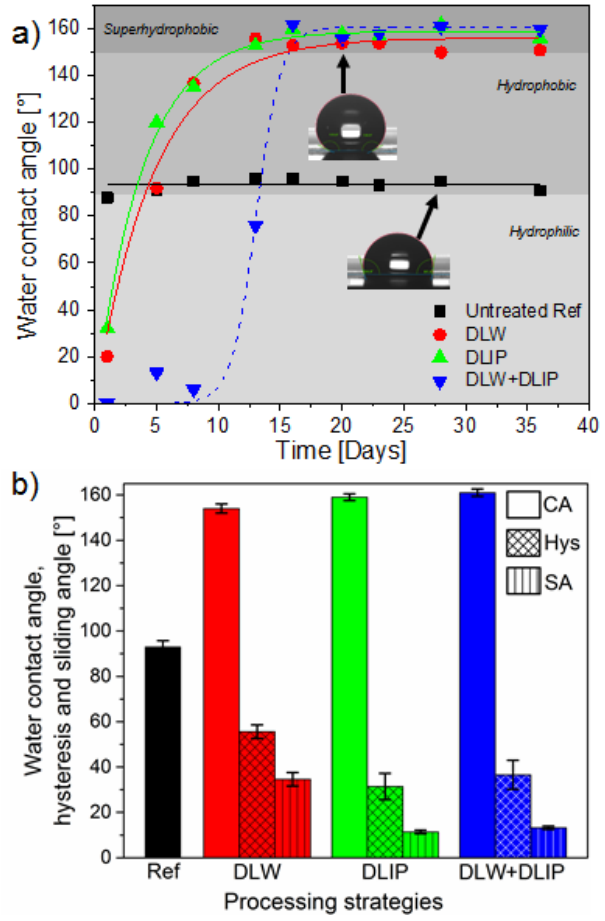


**Fig. 2.** Static water contact angle as a function of time of an untreated reference sample and of the laser processed samples, the fits are to guide the eye (a), the final contact angle after 95 days, the contact angle hysteresis and the sliding angle, respectively (b) [18].

Mostly responsible for this wetting state is, besides the surface chemistry, the fabricated topography which creates air cushions between the structure and the water droplet leading to the Cassie-Baxter wetting condition [18,29].
Besides the static contact angle, the wetting characteristic of a superhydrophobic surface was further analyzed by measuring the sliding angle (SA), which is the tilting angle of the substrate where the droplet starts to slide. In addition, also the contact angle hysteresis (Hys) was evaluated, defined as the difference between the advancing and the receding contact angle during the sliding of a droplet [30,31]. To evaluate the time-dependency of the reached superhydrophobic conditions, the static contact angle was measured again after 95 days. As shown in Fig. 2b, the CA of all laser treated samples remained above 150°. Additionally, the measured sliding angles were 34° for the DLW, 12° for DLIP and 13° for the hierarchical DLW+DLIP treated substrates. The contact angle hysteresis were 55° (DLW), 31° (DLIP) and 36° (DLW+DLIP), respectively (Fig. 2b) [18]. The significantly higher values for the DLW processed samples could indicate a Wenzel-controlled wetting regime instead of Cassie-Baxter [29]. For SA and Hys was not measureable for the untreated reference due to the static CA of 91°.

### 3.3 Self-cleaning efficiency

The method described in section 2.4 was applied for evaluating the self-cleaning efficiency of the different superhydrophobic surfaces.
In this case, the samples were contaminated with 1 µm manganese oxide particles ($MnO_2$) and held at a constant tilting angle of 15°. Then, 10 µl water droplets were deposited over the contaminated area. After each droplet rolled down the sample, the remaining relative contamination of manganese oxide particles was optically measured. The results are shown in Fig. 3. In the Fig. 3 insert, an SEM image of a single $MnO_2$ particle is shown.

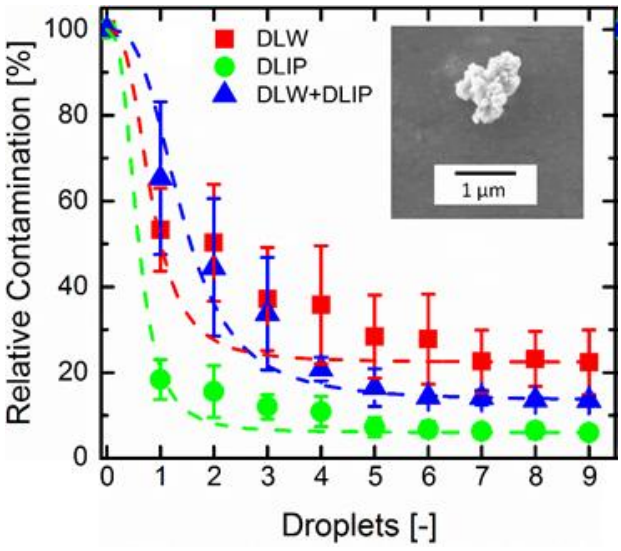


**Fig. 3.** Relative remaining contamination of 1 µm $MnO_2$ particles as a function of the released 10µl water droplets on the DLW, DLIP and DLW+DLIP structured surfaces for a tilting of the sample of 15°. The insert shows an SEM image of a single $MnO_2$ particle [20].

As it can be seen from Fig. 3, all surfaces showed a self-cleaning property due to the decrease of contamination as the droplets were sequentially released. However,

significant differences can be found between the laser treated surface. For instance, the number of remaining particles after the first droplet was 63%, 52% and 20% for the DLW+DLIP, DLW and DLIP treated samples, respectively. It should be emphasized that this is the contamination after the first droplet has passed the surface compared to the original contamination. The amount of particles was further reduced with an increasing number of droplets. The final contamination amount after 9 droplets, was 12% for DLW+DLIP, 21% for DLW and 6% for DLIP, showing again a better performance for the DLIP structures.
For the DLW treated Al samples, this behaviour could be partially explained due to the relative high Hys (55°) and an SA (34°) values (Fig. 2b).
For a more in-depth understanding of the interaction between the single particles and the laser-structured surfaces, SEM images of polluted substrates are shown in Fig. 4. As it can be seen, single particles as well as agglomerated particles are located at the large trenches of the DLW structures (Fig. 4a). In consequence, a single rolling droplet cannot reach into the deep DLW structures and pick up the trapped particles. This also explains why the amount of contamination after 9 droplets remains higher on the DLW structures compared to the DLIP structures, which have a shallower structure depth of 4.2 µm.

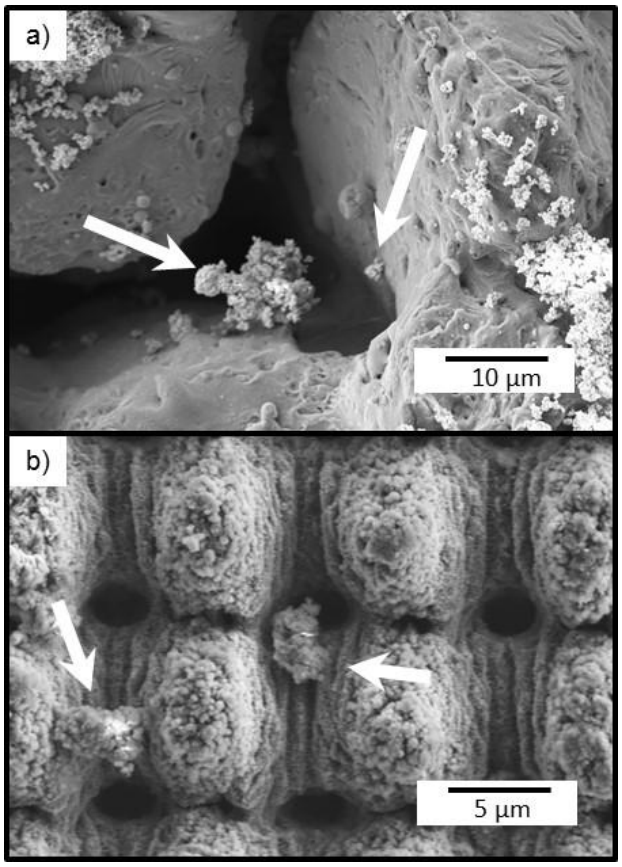


**Fig. 4.** SEM images of trenches between DLW-mesh (a) and DLIP pillar-like structures (b) contaminated with 1 µm $MnO_2$ particles. The arrows indicate single and agglomerated particles.

In contrast, the $MnO_2$ particles are not significantly trapped by DLIP structures (Fig. 4b) and they cannot agglomerate into big clusters due to the small spatial period of 7.0 µm. In addition, the superhydrophobic conditions are more pronounced in this sample, characaterized by a SA of 13° and a Hys of 31°.
The self-cleaning efficiency of the hierarchical DLW+DLIP structure lies between DLW and DLIP showing a 13% of contamination after the 9 water droplets.. Further test are require in the future in order to evaluate the influence of (i) particle's material and (ii) size, as well as (iii) the tilting angle and (iv) water droplet volume.

### 3.4 Ice-formation characterization

Since not all superhydrophobic surfaces show ice-repellent or anti-icing characteristics, the manufactured structures were tested regarding the formation of ice at a temperature of -20°C [8,18].
By plotting the freezing time as a function of the static CA (Fig. 5), a linear correlation regardless of the used laser-technology, and resulting topography, was observed, as it was already described elsewhere [32,33].
Two main factors explain this effect. First, an increase of the CA implies a reduction of the contact area between the droplet and the Al-surface. Therefore, leading to a lower heat transfer between both materials. In consequence, a delayed freezing process is observed (Fig. 5).
In addition to that, the air that is trapped between the structures and bootom droplet surface could also have an insulating effect. This hypothesis was evaluated by heat transfer simulations using FEM.

These results are also shown in Fig. 5, by the data ploted with a star-shape. The solid stars correspond to the simulation results assuming a structured surface with a spatial period of 50 µm and a structure height of 35 µm (comparable to the DLW mesh-like structure geometries), while the open stars shows the simulated freezing time considering that the surface is perfectly flat, i.e. the whole droplet bottom surface is in contact with the cold aluminium surface [18]. It is observed that the experimental data is satisfactorily followed by the numerical model, despite some fluctuations, probably due to deviations of the initial droplet volume from the nominal volume of 8 µl. The simulation results also suggest that the insulation effect by the trapped air has a minor influence on the freezing time and therefore can be neglected [18].

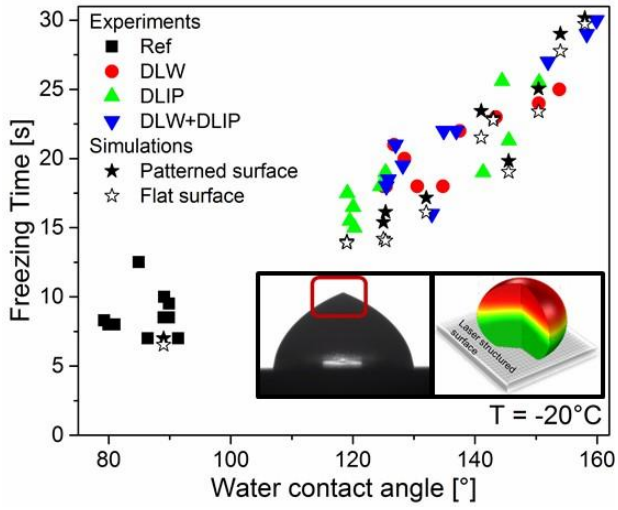


**Fig. 5.** Experimental and simulated freezing time of 8 µl droplets as a function of the static water contact angle at -20°C of patterned and flat surfaces. The left insert shows a frozen droplet on an untreated reference, the right insert depicts an impression of the heat transfer simulation inside a droplet.

Finally, an overview of the average freezing time of ten droplets placed onto each fabricated surface is presented in Fig. 6 (the error bars represent the respective standard deviation).

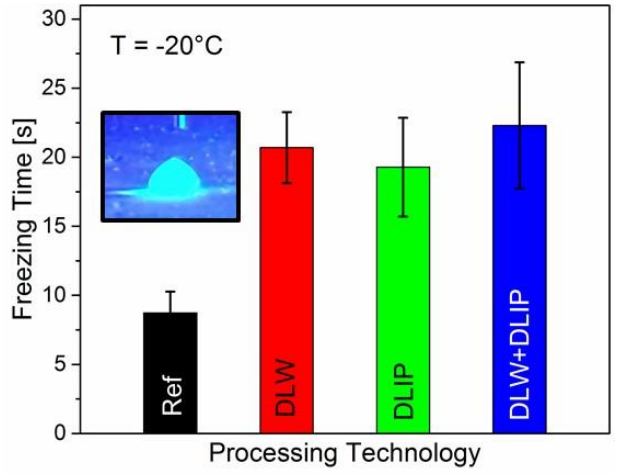


**Fig. 6.** Average freezing time of the droplets on an untreated reference, DLW, DLIP and DLW+DLIP structures at -20°C, the insert depicts the frozen droplet illuminated by the characterization machine.

The droplets froze the fastest on the untreated reference, after 8.7 s. Remarkably, droplets on the DLW+DLIP structure froze after 22.3 s, representing a nearly three-fold increase compared to the reference. The insert in Fig. 6 depicts an impression of a frozen 8 µl droplet on a reference sample illuminated by the drop shape analyzer.

## 4 Summary and conclusions

In this work, mesh-like, pillar-like, and multiscaled hierarchical structures were fabricated on pure aluminum using direct laser writing, direct laser interference patterning and a combination of both methods. The wetting characteristics were measured during 36 days period and revealed a superhydrophobic behavior for all laser structured samples with static water contact angles higher than 151° after at least 13 days. Additionally, the DLIP and DLW+DLIP treated substrates presented low sliding angles of 12° and 13°, respectively. This water repellent characteristic is closely linked to the effective self-cleaning property observed when the samples were covered with 1 µm manganese oxide particles and water droplets were let to roll down over the surface. Due to the significantly larger 50 µm mesh-like DLW structures, the contamination particles got trapped in between the trenches and agglomerated. Finally, the ice-repellent functionality at -20°C was demonstrated and the freezing time was increased from 8.7 up to 22.3 s for the hierarchical pattern.

This work was carried out in the framework of the Reinhart Koselleck project (323477257), which has received funding from the German Research Foundation (German: Deutsche Forschungsgemeinschaft DFG). The work of A.L. is also supported by the German Research Foundation (DFG) under Excellence Initiative program by the German federal and state government to promote top-level research at German universities. M. S. acknowledges the support of the Alexander von Humboldt Foundation.

## References

[1] H.J. Ensikat, P. Ditsche-Kuru, C. Neinhuis, and W. Barthlott, *Beilstein J. Nanotechnol.*, **2**, 152–161 (2011).
[2] P. Varshney, S.S. Mohapatra, and A. Kumar, *Biomimetics*, **2**, 2 (2017).
[3] J.G. Buijnsters, R. Zhong, N. Tsyntsaru, and J.-P. Celis, *ACS Appl. Mater. Interfaces*, **5**, 3224–3233 (2013).
[4] R. Liao, Z. Zuo, C. Guo, Y. Yuan, and A. Zhuang, *Applied Surface Science*, **317**, 701–709 (2014).
[5] J. Lomga, P. Varshney, D. Nanda, M. Satapathy, S.S. Mohapatra, and A. Kumar, *Journal of Alloys and Compounds*, **702**, 161–170 (2017).
[6] J. Zhu and X. Hu, *J Coat Technol Res*, **16**, 249–255 (2019).
[7] M.A. Ramadan, *Friction*, **6**, 457–463 (2018).
[8] M. Nosonovsky and V. Hejazi, *ACS Nano*, **6**, 8488–8491 (2012).
[9] T.Y. Zhao, P.R. Jones, and N.A. Patankar, *Sci Rep*, **9**, 1–12 (2019).
[10] M.J. Kreder, J. Alvarenga, P. Kim, and J. Aizenberg, *Nat Rev Mater*, **1**, 1–15 (2016).
[11] L.R. de Lara, R. Jagdheesh, and J.L. Ocaña, *Materials Letters*, **184**, 100–103 (2016).
[12] L. Gao, W. Zhou, Y. Wang, S. Wang, C. Bai, S. Li, B. Liu, J. Wang, and Y.L. Li, *Optik*, **127**, 5211–5214 (2016).
[13] C. Zwahr, B. Voisiat, A. Welle, D. Günther, and A.F. Lasagni, *Advanced Engineering Materials*, **20**, 1800160 (2018).
[14] F. Rößler, T. Kunze, and A.F. Lasagni, *Opt. Express, OE*, **25**, 22959–22970 (2017).
[15] R. Helbig, D. Günther, J. Friedrichs, F. Rößler, A. Lasagni, and C. Werner, *Biomaterials Science*, **4**, 1074–1078 (2016).

[16] B.-H. Ha, S. Ahn, H.-S. Bae, H.-S. Kang, J. Kim, and J. Noh, *Optics and Lasers in Engineering*, **107**, 214–220 (2018).
[17] S. Milles, B. Voisiat, M. Nitschke, and A.F. Lasagni, *Journal of Materials Processing Technology*, **270**, 142–151 (2019).
[18] S. Milles, M. Soldera, B. Voisiat, and A.F. Lasagni, *Sci Rep*, **9**, 1–13 (2019).
[19] A.I. Aguilar-Morales, S. Alamri, and A.F. Lasagni, *Journal of Materials Processing Technology*, **252**, 313–321 (2018).
[20] S. Milles, M. Soldera, T. Kuntze, and A.F. Lasagni, *In submission*, (2020).
[21] J.I. Ahuir-Torres, M.A. Arenas, W. Perrie, and J. de Damborenea, *Optics and Lasers in Engineering*, **103**, 100–109 (2018).
[22] A. Semerok, B. Sallé, J.-F. Wagner, and G. Petite, *Laser and Particle Beams*, **20**, 67–72 (2002).
[23] M. Bieda, M. Siebold, and A.F. Lasagni, *Applied Surface Science*, **C**, 175–182 (2016).
[24] B.N. Chichkov, C. Momma, S. Nolte, F. von Alvensleben, and A. Tünnermann, *Appl. Phys. A*, **63**, 109–115 (1996).
[25] K.-Y. Law, *J. Phys. Chem. Lett.*, **5**, 686–688 (2014).
[26] M. Thieme, R. Frenzel, S. Schmidt, F. Simon, A. Hennig, H. Worch, K. Lunkwitz, and D. Scharnweber, *Advanced Engineering Materials*, **3**, 691–695 (2001).
[27] E. Louvis, P. Fox, and C.J. Sutcliffe, *Journal of Materials Processing Technology*, **211**, 275–284 (2011).
[28] R. Jagdheesh, M. Diaz, and J.L. Ocaña, *RSC Adv.*, **6**, 72933–72941 (2016).
[29] A.B.D. Cassie and S. Baxter, *Trans. Faraday Soc.*, **40**, 546–551 (1944).
[30] E. Chibowski and F. Gonzalez-Caballero, *Journal of Adhesion Science and Technology*, **7**, 1195–1209 (1993).
[31] B. He, J. Lee, and N.A. Patankar, *Colloids and Surfaces A: Physicochemical and Engineering Aspects*, **248**, 101–104 (2004).
[32] S. Tabakova and F. Feuillebois, *Journal of Colloid and Interface Science*, **272**, 225–234 (2004).
[33] H. Zhang, Y. Zhao, R. Lv, and C. Yang, *International Journal of Thermal Sciences*, **101**, 59–67 (2016).